Supplementary Material to "Brain-based biotypes of psychiatric vulnerability in the acute aftermath of trauma"

1. Supplementary Methods

1.1 Psychometric assessment

Trauma severity was measured using an Injury Severity Score (ISS) which takes into account multiple injuries and anatomical regions based on the Abbreviated Injury Scale(Gennarelli & Wodzin, 2006). The AIS codes single injuries based by anatomic location and relative severity. Participants also rated their chance of dying during the index trauma on a scale of 0-10 (0 - "life was not threatened at all"; 10 - "came very close to being killed or easily could have been killed"). Participants were classified as experiencing head trauma if the individual reported hitting head, and being dazed, confused, or in a fog, or having amnesia for some of the event, or loss of consciousness (all individual self-report questions administered in the ED), following criteria for minor traumatic brain injury diagnosis according to the American Congress of Rehabilitation Medicine. General physical health status of the participant was assessed for the 30 days pre-trauma, with a derived normative score based on questions from the 12-Item Short Form Health Survey (SF-12)(Ware Jr, Kosinski, & Keller, 1996). The Childhood Trauma Questionnaire (CTQ) was administered 2 weeks post-trauma(Bernstein & Fink, 1998). This self-report measure assesses 5 types of childhood maltreatment: emotional abuse, physical abuse, sexual abuse, emotional neglect, and physical neglect. The AURORA study used an abbreviated version with 11 of the 28 items in the CTQ: 2 items each from the physical neglect, emotional neglect, emotional abuse, and physical abuse subtype and 3 items from the sexual abuse subtype. Items were summed to create a CTQ total score.

PTSD symptoms were assessed using the PTSD Symptom Checklist for DSM-5 (PCL-5)(Weathers et al., 2013). The PCL-5 is a 20 item self-report questionnaire assessing the presence and severity of hyperarousal, intrusions, negative cognitions, and avoidance symptoms. Each item was rated from 0 (not at all) to 4 (extremely), and items were summed to create a 0-80 scale. Depression symptoms were assessed using the Patient-Reported Outcomes Measurement Information System (PROMIS) Depression instrument (Pilkonis et al., 2011) with eight items evaluating depressive symptom frequency scored from 1 (never) to 5 (always). Items were summed and converted to a T-score. Dissociation was assessed using the Brief Dissociative Experiences Scale – Modified (DES-B)(Carlson & Putnam, 1993). The 8-item DES-B was abbreviated to include 2 items reflecting common forms of dissociation. Participants reported how often they had the following experiences: People, objects, or the world around you seemed strange or unreal, and You felt as though you were looking through a fog so that people and things seemed far away or unclear, on a scale of 1 (none of the time) - 5 (all or almost all of the time). The 2 items were summed to create a total dissociative experiences score. Impulsivity was assessed using the Impulsive Behavior Scale – Short Form (SUPPS-P; Cyders, Littlefield, Coffey & Karyadi, 2014). The 20-item scale was abbreviated to assess 8 items, measuring negative urgency, lack of perseverance items, lack of premeditation, and positive urgency, on a scale of 0 (never) to 4 (very often). A total SUPPS-P score was calculated by summing the items. Anxiety symptoms were assessed using 4 items from the PROMIS Anxiety bank (Pilonkis et al., 2011), assessing anxious feelings, worry, difficulty relaxing, and feeling tense, on a scale of 0 (none of the time) to 5 (all or almost all of the time).

Surveys were sent to participants via text or email for self-completion, or were completed with the assistance of telephone interviewers based on participant preference. All scales queried symptoms occurring in the past 2 weeks (2-week survey) or past 30 days (ED, 8-week, 3-month, and 6-month surveys). Missing values were imputed using multiple imputation in Hmisc v4.3, with 5 iterations of a 3-knot model, and missing values were replaced with values from the final iteration. N=7 participants missing data at all 4 timepoints were omitted from the analysis of mental health outcome trajectories; this appeared independent of subsequent biotyping assignments with n=2 each from clusters 1/2/4, and n=1 from cluster 3.

1.2 fMRI data processing and analyses

1.2.1 MRI data conversion and quality control. DICOM images were converted to NIFTI format with Brain Imaging Data Structure (BIDS) nomenclature using dcm2niix (Li et al. 2016) and were visually inspected for conversion errors and data exclusion criteria (e.g., signal drop-out from Falx calcification, anatomical abnormalities). Further quality control was achieved by running the MRIQC pipeline (version 0.10.4 in a Docker container) (Esteban et al. 2017a) on the structural and functional images.
Results included in this manuscript come from preprocessing performed using fMRIPrep 1.2.2 (Esteban, Blair, et al. (2017); Esteban, Markiewicz, et al. (2018); RRID:SCR_016216), which is based on Nipype 1.1.5 (Gorgolewski et al. (2011); Gorgolewski et al. (2017); RRID:SCR_002502). In order to maintain consistency in preprocessing throughout the duration of data collection, FMRIPrep was run in a Docker container retaining the version that was newest at the initiation of the study.

1.2.2 Anatomical data preprocessing. The T1-weighted (T1w) images were corrected for intensity non-uniformity using N4BiasFieldCorrection (Tustison et al. 2010, ANTs 2.2.0), and used as T1w-reference throughout the workflow. The T1w-reference was then skull-stripped using antsBrainExtraction.sh (ANTs 2.2.0), and OASIS as target template. Brain surfaces were reconstructed using recon-all (FreeSurfer 6.0.1, RRID:SCR_001847, Dale, Fischl, and Sereno 1999), and the brain mask estimated previously was refined with a custom variation of the method to reconcile ANTs-derived and FreeSurfer-derived segmentations of the cortical gray-matter of Mindboggle (RRID:SCR_002438, Klein et al. 2017). Spatial normalization to the ICBM 152 Nonlinear Asymmetrical template version 2009c (Fonov et al. 2009, RRID:SCR_008796) was performed through nonlinear registration with antsRegistration (ANTs 2.2.0, RRID:SCR_004757, Avants et al. 2008), using brain-extracted versions of both T1w volume and template. Brain tissue segmentation of cerebrospinal fluid (CSF), white-matter (WM) and gray-matter (GM) was performed on the brain-extracted T1w using fast (FSL 5.0.9, RRID:SCR_002823, Zhang, Brady, and Smith 2001).

1.2.3 Functional data preprocessing. For each of the 4 BOLD runs found per subject (across all tasks and sessions), the following preprocessing was performed. First, a reference volume and its skull-stripped version were generated using a custom methodology of fMRIPrep. The BOLD reference was then co-registered to the T1w reference using bbregister (FreeSurfer) which implements boundary-based registration (Greve and Fischl, 2009). Co-registration was configured with nine degrees of freedom to account for distortions remaining in the BOLD reference. Head-motion parameters with respect to the BOLD reference (transformation matrices, and six corresponding rotation and translation parameters) are estimated before any spatiotemporal filtering using mcflirt (FSL 5.0.9, Jenkinson et al. 2002). BOLD runs were slice-time corrected using 3dTshift from AFNI 20160207 (Cox, 1996, RRID:SCR_005927). The BOLD time-series (including slice-timing correction) were resampled onto their original, native space by applying a single, composite transform to correct for head-motion and susceptibility distortions. These resampled BOLD time-series will be referred to as ‘preprocessed BOLD in original space’, or just ‘preprocessed BOLD.’ First, a reference volume and its skull-stripped version were generated using a custom methodology of fMRIPrep. Automatic removal of motion artifacts using independent component analysis (ICA-AROMA, Pruim et al. 2015) was performed on the preprocessed BOLD on MNI space time-series after removal of non-steady state volumes and spatial smoothing with an isotropic, Gaussian kernel of 6mm FWHM (full-width half-maximum). To deal with cases in which motion was likely too high for effective ICA-based correction, we also implemented an overall motion threshold was set such that data from a particular task (Threat, Inhibition, Reward, Resting State) were excluded from analysis entirely for any participant with more than 15% of volumes exceeding 1mm FD.

Although not used in our current analyses, these regressors and corresponding non-denoised and unsmoothed images are available for alternative analyses in the future. These noise regressors were generated as follows:The BOLD time-series were resampled to MNI152NLin2009cAsym standard space, generating a preprocessed BOLD run in MNI152NLin2009cAsym space. First, a reference volume and its skull-stripped version were generated using a custom methodology of fMRIPrep. Several confounding time-series were calculated based on the preprocessed BOLD: framewise displacement (FD), DVARS and three region-wise global signals. FD and

DVARS are calculated for each functional run, both using their implementations in Nipype (following the definitions by Power et al. 2013). The three global signals are extracted within the CSF, the WM, and the whole-brain masks.

Additionally, a set of physiological regressors were extracted to allow for component-based noise correction (CompCor, Behzadi et al. 2007). Principal components are estimated after high-pass filtering the preprocessed BOLD time-series (using a discrete cosine filter with a 128s cut-off) for the two CompCor variants: temporal (tCompCor) and anatomical (aCompCor). Six tCompCor components are then calculated from the top 5% variable voxels within a mask covering the subcortical regions. This subcortical mask is obtained by heavily eroding the brain mask, which ensures it does not include cortical GM regions. For aCompCor, six components are calculated within the intersection of the aforementioned mask and the union of CSF and WM masks calculated in T1w space, after their projection to the native space of each functional run (using the inverse BOLD-to-T1w transformation). The head-motion estimates calculated in the correction step were also placed within the corresponding confounds file. The BOLD time-series, were resampled to surfaces on the following spaces: fsaverage5. All resamplings can be performed with a single interpolation step by composing all the pertinent transformations (i.e. head-motion transform matrices, susceptibility distortion correction when available, and co-registrations to anatomical and template spaces). Gridded (volumetric) resampling was performed using antsApplyTransforms (ANTs), configured with Lanczos interpolation to minimize the smoothing effects of other kernels (Lanczos 1964). Non-gridded (surface) resampling was performed using `mri_vol2surf`(FreeSurfer). Many internal operations of fMRIPrep use Nilearn 0.4.2 (Abraham et al. 2014, RRID:SCR_001362), mostly within the functional processing workflow.

1.2.4 First level models. Initial statistical modeling was conducted in SPM12. For the Threat task, blocks of fearful and neutral stimuli were modeled with separate boxcar functions representing the onset and 8000 ms duration of each block, convolved with a canonical hemodynamic response function. Contrasts of fearful>neutral face blocks were used for ROI extraction. For the Inhibition task, correct Go and correct No-Go trials were each modeled in an event-related design (0ms event duration), and incorrect Go and No-Go trials were modeled separately. Contrasts of correct No-Go > correct Go trials were used for ROI extraction. For the Reward task, gain and loss trials were modeled as separate experimental conditions in an event-related design, and any trial on which the participant neglected to make a button press was modeled in an error condition. Contrasts of Gain > Loss were used for ROI extraction. In all first-level models, white matter, CSF and global signal time courses were included as nuisance regressors, as this has been shown to provide a good balance of noise correction from motion/physiological sources while retaining signal quality, after ICA-AROMA (Satterthwaite et al., 2019).

1.2.5 Data extraction from regions of interest (ROIs). The mean across all voxels in each ROI was extracted from first-level contrasts using rex (https://www.nitrc.org/projects/rex/). ROIs were defined bilaterally, using anatomical boundaries. For Threat, ROIs included the amygdala(Tyszka & Pauli, 2016), insula(Tzourio-Mazoyer et al., 2002), and sgACC and dACC defined as Brodmann Areas 25 and 32 respectively, based on translational work showing that these are the primate cortical areas corresponding to regions that inhibit (BA 25) or express fear (BA 32)(Tang et al., 2019). For Reward, ROIs included the NAcc(Pauli, Nili, & Tyszka, 2018), OFC(Fischl et al., 2004), and amygdala(Tyszka & Pauli, 2016). For Inhibition, ROIs included the hippocampus(Hammers et al., 2003), and a 6mm sphere in vmPFC (centered at x=-4,y=44,z=-4) based on prior work with this task defining an area whose activation in the No-Go>Go contrast is correlated with inhibition of fear to unreinforced vs reinforced cues(Jovanovic et al., 2013). We did not require that all ROIs show significant task-related activation, as some regions with high inter-individual variability may not be significantly activated in group-level analyses.

Prior to clustering, fMRI data from each ROI were z-scored to minimize range effects. Outliers were replaced with a cap score at M±3SD. Scaling and outlier correction were conducted separately for discovery and replication cohorts. For the purpose of visualizing the cluster solutions, a principal components analysis (PCA) was conducted using factoextra 1.0.5. For the PCA, ROI data from both discovery and replication samples was

combined to allow the cluster solutions for discovery and replication to be displayed in the same latent variable space. Examination of the loadings (**Table S1**) indicated that the first three PCs corresponded to threat (23% of the variance), reward (21%), and inhibition (12%).

1.2.6 Whole-brain analyses. Whole brain analyses were conducted to identify task-related activation for the threat, reward, and inhibition tasks. Analyses were corrected for multiple comparisons using an initial voxel-wise threshold of $p<0.005$, in combination with an extent threshold for clusters to allow a family-wise error rate of less than 5% ($p_{FWE}<0.05$). The cluster extent thresholds required for this level of correction were k=114 for threat, k=82 for reward, and k=116 for inhibition. In addition, after having identified cluster solutions using the limited input data from the ROIs, we then conducted whole-brain ANOVAs to identify additional differences between cluster groups outside of the a priori ROIs (1 model per task). To meet a FWE-corrected $p<.05$, the initial cluster-forming threshold was again set to $p<.005$ and the extent thresholds were k=164 for threat, k=146 for reward, and no clusters meeting FWE-correction for the inhibition task.

1.3 Fear-potentiated startle

Fear-potentiated startle data were included to provide more insight into the individual differences seen in each of the clusters. Individuals with chronic PTSD show noted differences from trauma-exposed control participants during fear learning as well as extinction, including heightened fear to safety cues during fear acquisition, and slower extinction (Jovanovic et al., 2009). These features may be apparent in the early aftermath of trauma, potentially contributing to the prolonged maintenance of high levels of fear to trauma cues.

Psychophysiological data were collected at the same visit as the fMRI scan 2 weeks posttrauma, using a Pavlovian fear conditioning procedure (Glover et al., 2012; Jovanovic et al., 2009). The unconditioned stimulus (US) was a 140 psi airblast with a 250ms duration, delivered to the neck. Conditioned stimuli (CS) were colored shapes presented on a computer screen; the reinforced CS+ was paired with the US on 100% of the trials, and the non-reinforced CS- was never paired with the US. To assess the startle eyeblink response, a 108 dB white noise burst was presented during every CS trial, and during noise-alone (NA) trials for the assessment of baseline startle response. The startle probe was presented six seconds after CS onset, followed by the US 0.5 s later. Conditioning consisted of three blocks of four trials of each type (NA, CS+, CS-). After a 10-minute delay, extinction consisted of four blocks with four trials of each type (CS+, CS-, NA) wherein the US never occurred. The startle eyeblink response was measured using electromyography of the right orbicularis oculi muscle. Fear-potentiated startle was calculated by subtracting the startle magnitude to the noise probe alone from the startle magnitude to the CS in each block of the experiment.

The startle eyeblink response was measured using electromyography (EMG) of the right orbicularis oculi muscle using a Biopac MP150 (Biopac Systems, Inc., Aero Camino, CA). Two 5 mm Ag/AgCl pre-gelled disposable electrodes were placed 1 cm below the participant's pupil and 1 cm inferior to the lateral canthus. Impedances < 6 kOhm were accepted, and data was recorded at 1 kHz. Using MindWare software (MindWare Technologies, Inc.; Gahanna, OH), EMG signals were amplified by a gain of 2000 and visually inspected for artifact. Startle magnitude was defined as the maximal contraction 20 to 200 ms following the startle probe presentation. Fear-potentiated startle (FPS) was calculated by subtracting the startle magnitude to the noise probe alone from the startle magnitude to the CS in each block of the experiment, for both acquisition and extinction.

2. Supplemental Results

2.1 Demographic and pre-trauma characteristics of the four clusters

Because of the unconstrained clustering approach, key demographic features may differ across the clusters, potentially contributing to the cluster solution. There was no association between cluster assignment and age ($F_{2,121}$=0.45, p=.64), gender (χ^2 =0.38, p=.83), race/ethnicity (χ^2 =6.39, p=.38), educational attainment (χ^2 =23.44, p=.38), employment (χ^2 =5.95, p=.65), income (χ^2 =7.15, p=.71), BMI ($F_{2,121}$=0.23, p=.80), overall physical health prior to the trauma ($F_{2,119}$=1.39, p=.25), marital status (χ^2 =5.52, p=.70), or childhood trauma exposure ($F_{2,121}$=0.86, p=.43). There was also no association between cluster assignment and features of the index trauma such as trauma type (χ^2 =14.36, p=.57), participants' assessment of chance of dying ($F_{2,121}$=2.19, p=.12), or injury severity ($F_{2,121}$=1.25, p=.29). There were no differences in head trauma across clusters, χ^2 = 1.08, p=.58. There was no relationship with the site of the MRI data collection, χ^2 =4.59, p=.60, nor aspects of data quality for any of the three fMRI scans (**ST2**). Finally, there were no cluster-wise differences in the proportion of participants taking medications, or psychiatric medications specifically (**ST5**). The clusters therefore appear to reflect covert neurocognitive features, rather than demographic, health-related, trauma-related, or site-specific factors.

Table S1. Principal Components Analysis for dataset including Cohort 1 + 2 – factor loadings

Task	ROI	PC1 (0.23) [a]	PC2 (0.21)	PC3 (0.12)	PC4 (0.11)	PC5 (0.09)	PC6 (0.08)	PC7 (0.06)	PC8 (0.06)	PC9 (0.04)
Threat	Amygdala	0.35	0.00	0.14	0.31	-0.37	0.29	0.72	-0.09	0.15
	Insula	0.54	0.15	0.17	-0.29	0.35	-0.19	-0.02	0.15	0.62
	dACC	0.56	0.12	0.05	-0.07	0.20	-0.22	0.09	0.04	-0.75
	sgACC	0.44	-0.27	0.11	0.39	-0.17	0.31	-0.65	-0.13	0.04
Inhibition	Hippocampus	-0.25	-0.04	0.67	0.49	0.49	-0.09	0.08	-0.01	-0.03
	vmPFC	-0.06	-0.24	0.66	-0.59	-0.35	0.04	-0.04	-0.12	-0.11
Reward	Nacc	-0.03	0.46	0.20	0.24	-0.53	-0.40	-0.18	0.46	0.02
	Amygdala	-0.06	0.49	0.12	-0.15	0.16	0.75	-0.08	0.34	-0.11
	OFC	-0.01	0.61	0.06	0.00	-0.05	-0.05	-0.11	-0.78	0.04

[a] Component (% variance in the original data accounted for by that component)

Table S2. Analysis of cluster associations with MRI data quality, by fMRI task

Task	FD	DVARS	TSNR
Threat	$F_{1,121}$=1.17, p=0.31	$F_{1, 121}$=0.90, p=0.41	$F_{1, 121}$=0.33, p=0.72
Inhibition	$F_{1, 121}$=1.11, p=0.33	$F_{1, 121}$=0.14, p=0.86	$F_{1, 121}$=0.31, p=0.73
Reward	$F_{1, 121}$=0.10, p=0.90	$F_{1, 121}$=0.10, p=0.90	$F_{1, 121}$=0.29, p=0.75

Abbreviations: FD- Framewise displacement, DVARS- Standard deviation in the global signal, TSNR- Temporal signal-to-noise ratio

Table S3. Model fit (QICC[a]) for cluster-based versus dimensional fMRI predictors of post-trauma outcome

Outcome	β PC1/PC2/PC3	Dimensional model, QIC	Cluster-based model, QIC
PTSD	1.21/0.63/-3.58	127153.83	129606.88
Depression	0.20/0.70/-1.80	49842.45	50801.76
Dissociation	0.14/-0.25/-0.65*	1574.94	1564.82
Anxiety	0.60/-0.10/-0.82	8911.06	9379.86
Impulsivity	1.21/0.63/-3.58, all n.s.	8680.61	8665.33

[a] QICC- Corrected Quasi Likelihood under Independence Model Criterion. Smaller values indicate better model fit
* = p<0.05.

Table S4. Whole-brain comparisons of the four groups

Task	Group comparison	Region	HEM	x	y	z	Z	Volume (mm3)
Threat (Fearful > Neutral Faces)	1 > (2, 4)	Mid. Cingulate G.	L	-4	-14	42	6.30	110916
		Mid. Cingulate G.	R	10	24	36	5.86	
		Supp. Motor Area	R	2	14	46	5.45	
		Fusiform G., Hypothalamus, Occipital, Insula	R	22	-34	-16	5.86	563436
		Rolandic Oper.	R	62	-10	12	5.57	
		Sup. Temporal G.	L	-38	-24	0	5.46	
		Ventral Tegmental Area	L	-2	-26	-22	5.24	5022
		Median Raphe Nucleus	R	4	-22	-28	4.25	
		Mesopontine	L	-10	-20	-28	4.19	
		Cuneus	L	-14	-78	30	4.47	6210
		Cuneus	L	-12	-70	22	3.31	
		Cuneus	L	-6	-82	36	3.23	
		Inf. Occipital G.	L	-50	-68	-12	4.39	6804
		Inf. Temporal G.	L	-54	-58	-6	3.88	
		Inf. Occipital G.	L	-44	-76	-4	3.75	
		Sup. Occipital G.	R	22	-64	48	4.28	8532
		Sup. Parietal G.	R	32	-64	52	3.70	
		Sup. Occipital G.	R	26	-60	40	3.52	
		Caudate	L	-8	10	16	4.13	8370
		Caudate	R	4	8	8	4.06	
		Thalamus	L	-12	-4	4	3.95	
		Sup. Frontal G.	L	-22	12	62	4.05	7263
		Sup. Frontal G.	L	-20	20	52	3.47	
		Supp. Motor Area	L	-6	6	60	3.44	
		Sup. Frontal G.	L	-16	58	30	4.02	4833
		Sup. Frontal G.	L	-4	62	28	3.77	
		Sup. Frontal G.	L	-30	54	26	3.51	
	2 > (1, 4)	Parahippocampal G.	R	22	-16	-22	4.55	5292
		Amygdala	R	24	-4	-16	4.16	
		Parahippocampal G.	R	16	-6	-20	3.29	
		Rolandic Oper.	R	54	-2	6	4.29	9153
		Insula	R	44	0	-6	3.67	
		Temporal Pole	R	60	4	2	3.31	
		Mid. Temporal G.	L	-42	-14	-16	4.25	7047
		Hippocampus	L	-28	-16	-20	3.50	
		Parahippocampal G.	L	-18	-12	-24	3.40	
		Supramarginal G.	L	-58	-38	28	3.68	4428

		Sup. Temporal G.	L	-44	-32	18	3.63	
		Insula	L	-32	-20	12	3.30	
	4 > (1, 2)	* No significant clusters						
Reward (Monetary Gain > Loss)	1 > (2, 4)	Caudate	R	8	8	-6	5.07	12069
		Caudate	L	-18	24	0	4.03	
		Putamen	R	20	4	-8	4.01	
		Ant. Cingulate G.	L	-6	42	12	4.82	40284
		Orbitofrontal G.	L	-8	40	-10	4.80	
		Ant. Cingulate G.	R	14	40	16	4.64	
		Fusiform G.	L	-34	-26	-18	4.76	3942
		Fusiform G.	L	-34	-40	-22	4.63	
		Fusiform G.	L	-30	-36	-16	3.17	
		Sup. Temporal G.	R	66	-6	6	4.72	25326
		Insula	R	48	14	-10	4.68	
		Rolandic Oper.	R	36	-20	18	4.59	
		Heschl G.	L	-36	-24	14	4.50	25083
		Postcentral G.	L	-66	-4	26	4.25	
		Postcentral G.	L	-64	-20	18	4.24	
		Precuneus	L	-12	-52	46	4.41	10044
		Sup. Parietal G.	L	-20	-60	54	4.34	
		Precuneus	L	-2	-44	40	3.75	
		Angular G.	L	-50	-60	24	4.20	8505
		Angular G.	L	-46	-72	42	3.93	
		Angular G.	L	-52	-70	36	3.58	
		Parahippocampal	R	20	-16	-22	4.15	3942
		Parahippocampal	R	12	-22	-26	3.47	
		Hippocampus	R	32	-10	-20	3.26	
		Mid. Cingulate G.	--	0	-2	36	3.98	4995
		Mid. Cingulate G.	R	12	-16	40	3.81	
		Mid. Cingulate G.	--	0	-18	36	3.34	
		Precuneus	R	12	-44	60	3.54	4077
		Precuneus	R	6	-38	56	3.50	
		Paracentral lobule	R	14	-40	48	2.88	
	2 > (1, 4)	* No significant clusters						
	4 > (1, 3)	* No significant clusters						
Inhibition (No-Go > Go)	No differences							

across groups						

Table S5. MRI scan sequence parameters by site

	SITE1 SIEMENS TIM 3T TRIO (12 CHANNEL HEAD COIL)	**SITE2 SIEMENS TIM 3T TRIO (12 CHANNEL HEAD COIL)**	**SITE3 SIEMENS MAGNETOM 3T PRISMA (20 CHANNEL HEAD COIL)**	**SITE4 SIEMENS 3T VERIO (12 CHANNEL HEAD COIL)**
MODALITY				
T1-WEIGHTED	**TR** = 2530ms, **TEs** = 1.74/3.6/5.46/7.32ms, **TI** = 1260ms, **flip angle** = 7, **FOV** = 256mm, **slices** = 176, **Voxel size** = 1mm x 1mm x 1mm	**TR** = 2530ms, **TEs** = 1.74/3.6/5.46/7.32ms, **TI** = 1260ms, **flip angle** = 7, **FOV** = 256mm, **slices** = 176, **Voxel size** = 1mm x 1mm x 1mm	**TR** = 2300ms, **TE** = 2.96ms, **TI** = 900ms, **flip angle** = 9, **FOV** = 256mm, **slices** = 176, **Voxel size** = 1.2mm x 1.0mm x 12mm	**TR** = 2530ms, **TEs** = 1.74/3.65/5.51/7.72ms, **TI** = 1260ms, **flip angle** = 7, **FOV** = 256mm, **slices** = 176, **Voxel size** = 1mm x 1mm x 1mm
FUNCTIONAL MRI	**TR** = 2360ms, **TE** = 30ms, **flip angle** = 70, **FOV** = 212mm, **slices** = 44, **Voxel size** = 3mm x 2.72mm x 2.72mm, 0.5 mm gap	**TR** = 2360ms, **TE** = 30ms, **flip angle** = 70, **FOV** = 212mm, **slices** = 44, **Voxel size** = 3mm x 3mm x 3mm, 0.5 mm gap	**TR** = 2360ms, **TE** = 29ms, **flip angle** = 70, **FOV** = 212mm, **slices** = 44, **Voxel size** = 3mm x 2.72mm x 2.72mm, 0.5 mm gap	**TR** = 2360ms, **TE** = 30ms, **flip angle** = 70, **FOV** = 212mm, **slices** = 42, **Voxel size** = 3mm x 2.72mm x 2.72mm, 0.5 mm gap

Table S6. Medications taken at any point post-trauma, by cluster (N)

Medication type	Cluster 1	Cluster 2	Cluster 3	Cluster 4	Total
Acetaminophen	1	4	0	1	6
ACE Inhibitors	3	3	2	0	8
Antibiotics	1	2	1	2	6
Anticholinergics	1	7	0	2	10
Benzodiazepines	0	3	1	1	5
Beta blockers	0	2	0	0	2
Contraceptives	1	1	0	1	3
Non-steroidal anti-inflammatory	6	11	3	5	25
Opioids	2	2	0	4	8
Serotonin and norepinephrine reuptake inhibitors	1	1	1	1	4
Serotonin reuptake inhibitors	1	5	0	3	9
Any medication χ^2 =0.62, p=0.89 with Cluster 3 χ^2 =0.41, p=0.81 without Cluster 3	**10**	**21**	**6**	**11**	**48**
Any psychoactive medication χ^2 =2.40, p=0.49 with Cluster 3 χ^2 =1.72, p=0.42 without Cluster 3	**4**	**9**	**2**	**7**	**22**

Figure S1 Cluster number metrics for fMRI data collected 2 weeks post-trauma, for the discovery sample (a-b) and replication sample (c-d).
(**a,b**) Weighted sum of squares for within-cluster point distances across a range of cluster solutions. The optimal solution following Hartigan's distance index is denoted with dotted line. (**c,d**) Silhouette width for a range of cluster solutions after hierarchical clustering using Wilk's criterion. Width summarizes the distance of points within a cluster relative to points outside the cluster. Dotted line indicates maximum silhouette width.

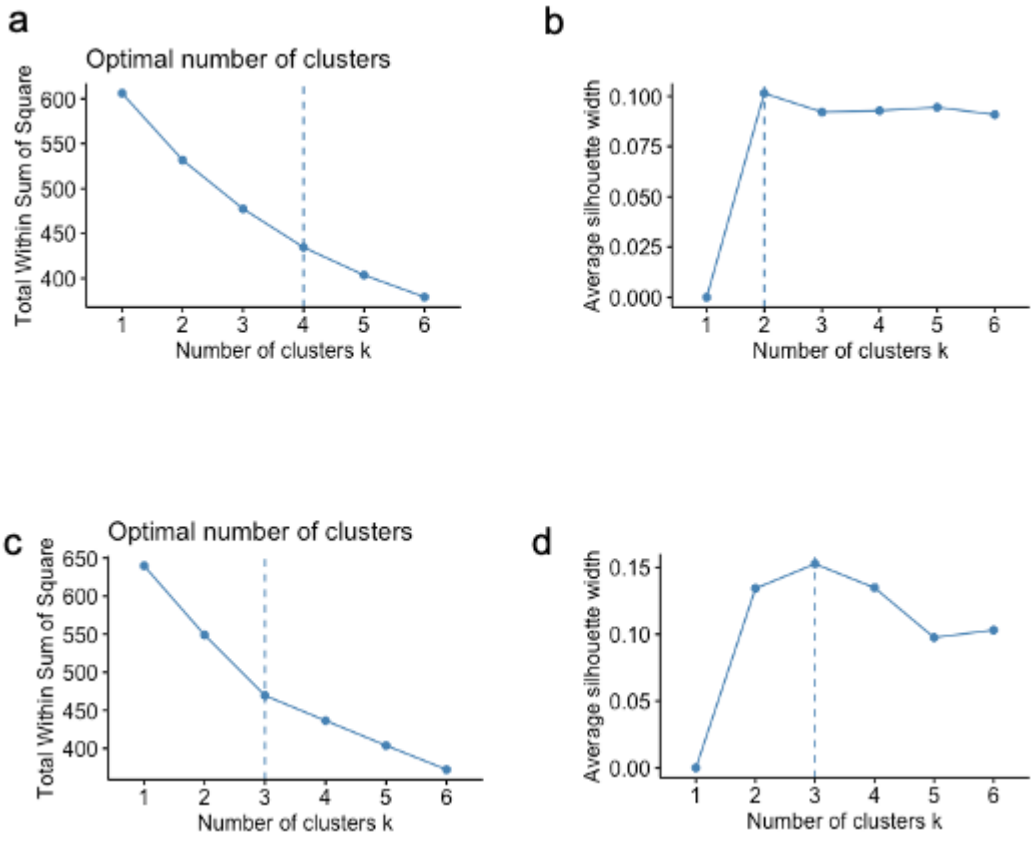

Figure S2 Amygdala reactivity to threat after traumas producing different levels of injury severity. Greater injury severity was linked with greater amygdala reactivity to threat, $F_{1,144}=4.58$, $p=0.03$.

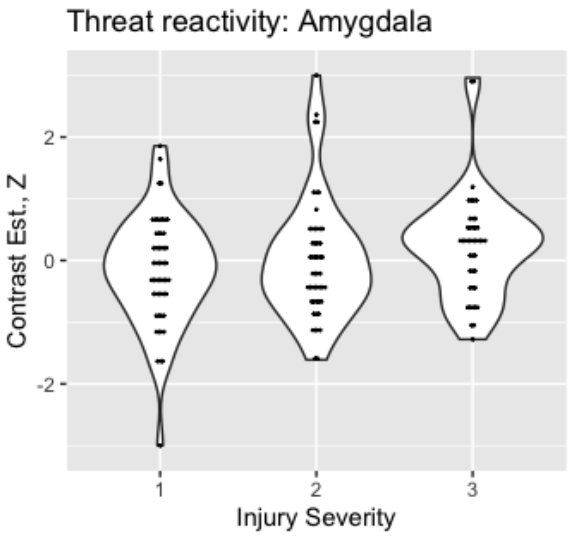

Figure S3. Sitewise differences in quality assurance metrics. Differences in framewise displacement (FD), standard deviation in the global signal (DVARs), and temporal signal-to-noise ratio (TSNR) were calculated between each neuroimaging site. Black bars reflect the mean value of each metric per site, and dots illustrate each participant of the combined n=146 (discovery + replication cohorts).

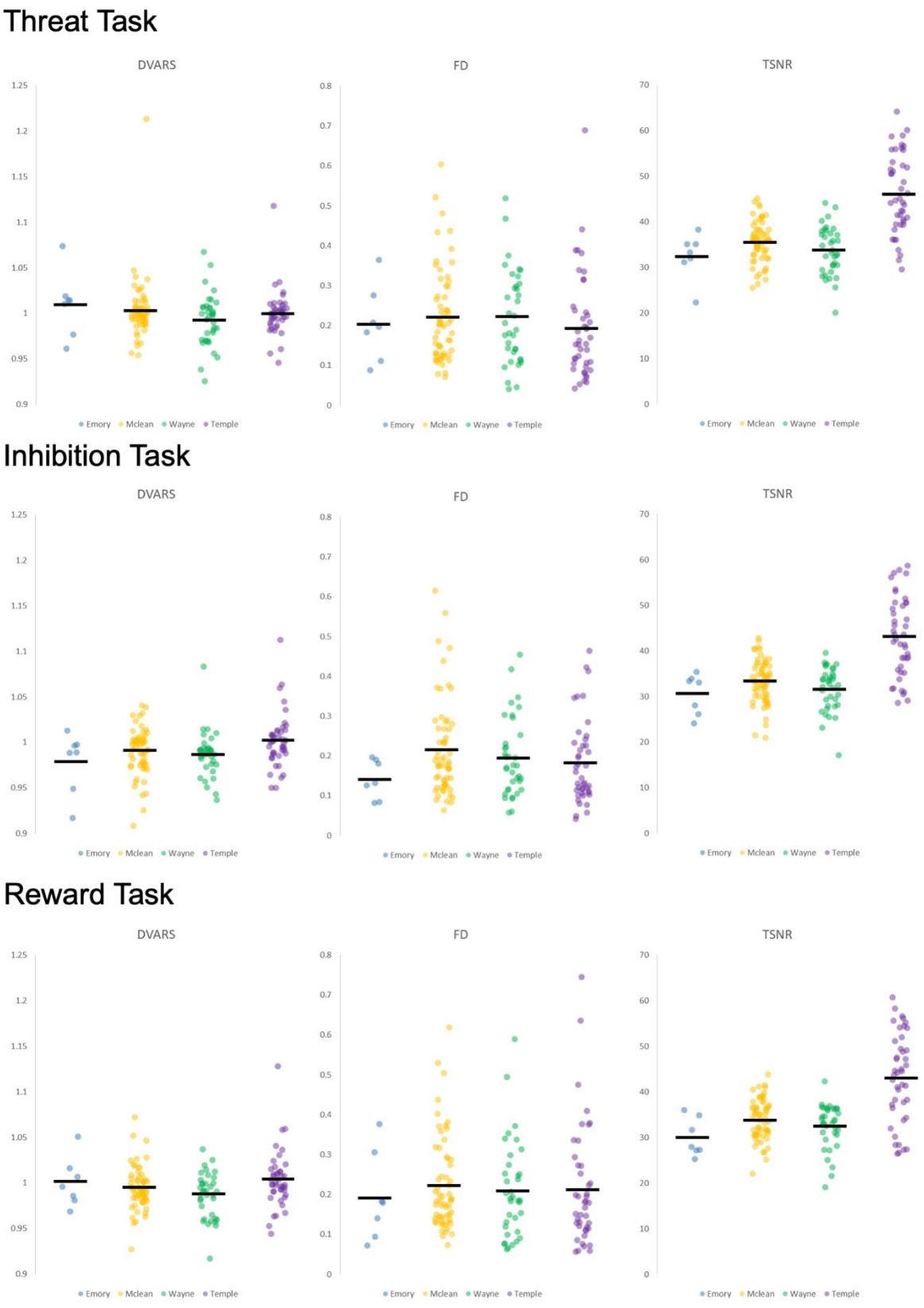

References

Abraham A, Pedregosa F, Eickenberg M, Gervais P, Mueller A, Kossaifi J, Gramfort A, Thirion B, Varoquaux G. Machine learning for neuroimaging with scikit-learn. Front in Neuroinf 8:14. 2014. doi:10.3389/fninf.2014.00014.

Andersson, J L R, Jenkinson, M., & Smith, S. (2007). Non-linear registration aka spatial normalisation. FMRIB Technical Report TRO7JA2. Retrieved from http://fmrib.medsci.ox.ac.uk/analysis/techrep/tr07ja2/tr07ja2.pdf

Andersson, Jesper L.R., & Sotiropoulos, S. N. (2016). An integrated approach to correction for off-resonance effects and subject movement in diffusion MR imaging. NeuroImage, 125, 1063–1078. https://doi.org/10.1016/j.neuroimage.2015.10.019

Avants BB, Epstein CL, Grossman M, Gee JC. Symmetric diffeomorphic image registration with cross-correlation: evaluating automated labeling of elderly and neurodegenerative brain. Med Image Anal. 2008 Feb;12(1):26–41. doi:10.1016/j.media.2007.06.004.

Behzadi Y, Restom K, Liau J, Liu TT. A component based noise correction method (CompCor) for BOLD and perfusion based fMRI. Neuroimage. 2007 Aug 1;37(1):90–101. doi:10.1016/j.neuroimage.2007.04.042.

Bernstein, D. P., & Fink, L. (1998). Childhood trauma questionnaire: A retrospective self-report: Manual: Psychological Corporation.

Carlson, E. B., & Putnam, F. W. (1993). An update on the dissociative experiences scale. Dissociation: progress in the dissociative disorders.

Cox RW. AFNI: software for analysis and visualization of functional magnetic resonance neuroimages. Comput Biomed Res. 1996 Jun;29(3):162–73. doi:10.1006/cbmr.1996.0014.

Cyders, M.A., Littlefield, A.K., Coffey, S., Karyadi, K.A. (2014). Examination of a short English version of the UPPS-P Impulsive Behavior Scale. Addictive Behaviors, 39(9), 1372-1376.

Dale A, Fischl B, Sereno MI. Cortical Surface-Based Analysis: I. Segmentation and Surface Reconstruction. Neuroimage. 1999;9(2):179–94. doi:10.1006/nimg.1998.0395.

Esteban O, Birman D, Schaer M, Koyejo OO, Poldrack RA, Gorgolewski KJ; MRIQC: Advancing the Automatic Prediction of Image Quality in MRI from Unseen Sites; PLOS ONE. September 2017; 12(9):e0184661; doi:10.1371/journal.pone.0184661.

Esteban, O., Blair, R., Markiewicz, C. J., Berleant, S. L., Moodie, C., Ma, F., ... & Poldrack, R. A. poldracklab/fmriprep: 1.0. 0-rc10, November 2017. URL https://doi. org/ 10.5281/zenodo.852659.

Esteban O, Markiewicz CJ, Blair RW, Moodie CA, Isik AI, Erramuzpe A, Kent JD, Goncalves M, DuPre E, Snyder M, Oya H, Ghosh SS, Wright J, Durnez J, Poldrack RA, Gorgolewski KJ. fMRIPrep: a robust preprocessing pipeline for functional MRI. Nat Meth. 2018; doi:10.1038/s41592-018-0235-4

Fischl, B., Van Der Kouwe, A., Destrieux, C., Halgren, E., Ségonne, F., Salat, D. H., . . . Kennedy, D. (2004). Automatically parcellating the human cerebral cortex. Cerebral Cortex, 14(1), 11-22.

Fonov VS, Evans AC, McKinstry RC, Almli CR, Collins DL. Unbiased nonlinear average age-appropriate brain templates from birth to adulthood. NeuroImage; Amsterdam. 2009 Jul 1;47:S102. doi:10.1016/S1053-8119(09)70884-5.

Gennarelli, T. A., & Wodzin, E. (2006). AIS 2005: a contemporary injury scale. Injury, 37(12), 1083-1091. doi:10.1016/j.injury.2006.07.009

Glover, E. M., Jovanovic, T., Mercer, K. B., Kerley, K., Bradley, B., Ressler, K. J., & Norrholm, S. D. (2012). Estrogen levels are associated with extinction deficits in women with posttraumatic stress disorder. Biol Psychiatry, 72(1), 19-24. doi:10.1016/j.biopsych.2012.02.031

Gorgolewski K, Burns CD, Madison C, Clark D, Halchenko YO, Waskom ML, Ghosh SS. Nipype: a flexible, lightweight and extensible neuroimaging data processing framework in python. Front Neuroinform. 2011 Aug 22;5(August):13. doi:10.3389/fninf.2011.00013.

Gorgolewski KJ, Esteban O, Ellis DG, Notter MP, Ziegler E, Johnson H, Hamalainen C, Yvernault B, Burns C, Manhães-Savio A, Jarecka D, Markiewicz CJ, Salo T, Clark D, Waskom M, Wong J, Modat M, Dewey BE, Clark MG, Dayan M, Loney F, Madison C, Gramfort A, Keshavan A, Berleant S, Pinsard B, Goncalves M, Clark D, Cipollini B, Varoquaux G, Wassermann D, Rokem A, Halchenko YO, Forbes J, Moloney B, Malone IB, Hanke M, Mordom D, Buchanan C, Pauli WM, Huntenburg JM, Horea C, Schwartz Y, Tungaraza R, Iqbal S, Kleesiek J, Sikka S, Frohlich C, Kent J, Perez-Guevara M, Watanabe

A, Welch D, Cumba C, Ginsburg D, Eshaghi A, Kastman E, Bougacha S, Blair R, Acland B, Gillman A, Schaefer A, Nichols BN, Giavasis S, Erickson D, Correa C, Ghayoor A, Küttner R, Haselgrove C, Zhou D, Craddock RC, Haehn D, Lampe L, Millman J, Lai J, Renfro M, Liu S, Stadler J, Glatard T, Kahn AE, Kong X-Z, Triplett W, Park A, McDermottroe C, Hallquist M, Poldrack R, Perkins LN, Noel M, Gerhard S, Salvatore J, Mertz F, Broderick W, Inati S, Hinds O, Brett M, Durnez J, Tambini A, Rothmei S, Andberg SK, Cooper G, Marina A, Mattfeld A, Urchs S, Sharp P, Matsubara K, Geisler D, Cheung B, Floren A, Nickson T, Pannetier N, Weinstein A, Dubois M, Arias J, Tarbert C, Schlamp K, Jordan K, Liem F, Saase V, Harms R, Khanuja R, Podranski K, Flandin G, Papadopoulos Orfanos D, Schwabacher I, McNamee D, Falkiewicz M, Pellman J, Linkersdörfer J, Varada J, Pérez-García F, Davison A, Shachnev D, Ghosh S. Nipype: a flexible, lightweight and extensible neuroimaging data processing framework in Python. 2017. doi:10.5281/zenodo.581704.

Greve DN, Fischl B. Accurate and robust brain image alignment using boundary-based registration. Neuroimage. 2009 Oct;48(1):63–72. doi:10.1016/j.neuroimage.2009.06.060.

Hammers, A., Allom, R., Koepp, M. J., Free, S. L., Myers, R., Lemieux, L., . . . Duncan, J. S. (2003). Three-dimensional maximum probability atlas of the human brain, with particular reference to the temporal lobe. Human Brain Mapping, 19(4), 224-247. Retrieved from https://onlinelibrary.wiley.com/doi/full/10.1002/hbm.10123

Iglesias, J. E., Liu, C. Y., Thompson, P. M., & Tu, Z. (2011). Robust brain extraction across datasets and comparison with publicly available methods. IEEE Transactions on Medical Imaging, 30(9), 1617–1634. https://doi.org/10.1109/TMI.2011.2138152

Jenkinson M, Bannister P, Brady M, Smith S. Improved optimization for the robust and accurate linear registration and motion correction of brain images. Neuroimage. 2002 Oct;17(2):825–41. doi:10.1006/nimg.2002.1132.

Jovanovic, T., Blanding, N. Q., Norrholm, S. D., Duncan, E., Bradley, B., & Ressler, K. J. (2009). Childhood abuse is associated with increased startle reactivity in adulthood. Depress Anxiety, 26(11), 1018-1026. doi:10.1002/da.20599

Jovanovic, T., Ely, T., Fani, N., Glover, E. M., Gutman, D., Tone, E. B., . . . Ressler, K. J. (2013). Reduced neural activation during an inhibition task is associated with impaired fear inhibition in a traumatized civilian sample. Cortex, 49(7), 1884-1891. doi:10.1016/j.cortex.2012.08.011

Klein A, Ghosh SS, Bao FS, Giard J, Häme Y, Stavsky E, et al. Mindboggling morphometry of human brains. PLoS Comput Biol 13(2): e1005350. 2017. doi:10.1371/journal.pcbi.1005350.

Lanczos, C. (1964). Evaluation of noisy data. Journal of the Society for Industrial and Applied Mathematics, Series B: Numerical Analysis, 1(1), 76-85.

Leon, A. C., Olfson, M., Portera, L., Farber, L., & Sheehan, D. V. (1997). Assessing psychiatric impairment in primary care with the Sheehan Disability Scale. The international journal of psychiatry in medicine, 27(2), 93-105. Retrieved from https://journals.sagepub.com/doi/abs/10.2190/T8EM-C8YH-373N-1UWD

Li X, Morgan PS, Ashburner J, Smith J, Rorden C (2016) The first step for neuroimaging data analysis: DICOM to NIfTI conversion. J Neurosci Methods. 264:47-56. doi: 10.1016/j.jneumeth.2016.03.001. PMID: 26945974

Orben, A., & Lakens, D. Crud (Re)Defined. Advances in Methods and Practices in Psychological Science, 0(0), 2515245920917961. doi:10.1177/2515245920917961

Pauli, W. M., Nili, A. N., & Tyszka, J. M. (2018). A high-resolution probabilistic in vivo atlas of human subcortical brain nuclei. Scientific data, 5, 180063.

Pilkonis, P. A., Choi, S. W., Reise, S. P., Stover, A. M., Riley, W. T., Cella, D., & Group, P. C. (2011). Item banks for measuring emotional distress from the Patient-Reported Outcomes Measurement Information System (PROMIS®): depression, anxiety, and anger. Assessment, 18(3), 263-283.

Power JD, Mitra A, Laumann TO, Snyder AZ, Schlaggar BL, Petersen SE. Methods to detect, characterize, and remove motion artifact in resting state fMRI. Neuroimage. 2013 Aug 29;84:320–41. doi:10.1016/j.neuroimage.2013.08.048.

Pruim RHR, Mennes M, van Rooij D, Llera A, Buitelaar JK, Beckmann CF. ICA-AROMA: A robust ICA-based strategy for removing motion artifacts from fMRI data. Neuroimage. 2015 May 15;112:267–77. doi:10.1016/j.neuroimage.2015.02.064.

Roalf, D. R., Quarmley, M., Elliott, M. A., Satterthwaite, T. D., Vandekar, S. N., Ruparel, K., ... & Prabhakaran, K. (2016). The impact of quality assurance assessment on diffusion tensor imaging outcomes in a large-scale population-based cohort. Neuroimage, 125, 903-919.

Satterthwaite, T. D., Ciric, R., Roalf, D. R., Davatzikos, C., Bassett, D. S., & Wolf, D. H. (2019). Motion artifact in studies of functional connectivity: Characteristics and mitigation strategies. Human Brain Mapping, 40(7), 2033-2051. Retrieved from https://www.ncbi.nlm.nih.gov/pmc/articles/PMC5930165/pdf/nihms878475.pdf

Sheehan, D. V., Harnett-Sheehan, K., & Raj, B. A. (1996). The measurement of disability. Int Clin Psychopharmacol, 11 Suppl 3, 89-95. doi:10.1097/00004850-199606003-00015

Smith, S. M., Jenkinson, M., Woolrich, M. W., Beckmann, C. F., Behrens, T. E. J., Johansen-Berg, H., … Matthews, P. M. (2004). Advances in functional and structural MR image analysis and implementation as FSL. In NeuroImage (Vol. 23). https://doi.org/10.1016/j.neuroimage.2004.07.051

Tang, W., Jbabdi, S., Zhu, Z., Cottaar, M., Grisot, G., Lehman, J. F., . . . Haber, S. N. (2019). A connectional hub in the rostral anterior cingulate cortex links areas of emotion and cognitive control. eLife, 8, e43761. doi:10.7554/eLife.43761

Tustison NJ, Avants BB, Cook PA, Zheng Y, Egan A, Yushkevich PA, Gee JC. N4ITK: improved N3 bias correction. IEEE Trans Med Imaging. 2010 Jun;29(6):1310–20. doi:10.1109/TMI.2010.2046908.

Tyszka, J. M., & Pauli, W. M. (2016). In vivo delineation of subdivisions of the human amygdaloid complex in a high-resolution group template. Human Brain Mapping, 37(11), 3979-3998.

Tzourio-Mazoyer, N., Landeau, B., Papathanassiou, D., Crivello, F., Etard, O., Delcroix, N., . . . Joliot, M. (2002). Automated anatomical labeling of activations in SPM using a macroscopic anatomical parcellation of the MNI MRI single-subject brain. Neuroimage, 15(1), 273-289. Retrieved from http://www.sciencedirect.com/science/article/B6WNP-4575RNN-1F/2/3d7eadc4477a1a64629325332495df1d

Wang, S., Peterson, D. J., Gatenby, J. C., Li, W., Grabowski, T. J., & Madhyastha, T. M. (2017). Evaluation of field map and nonlinear registration methods for correction of susceptibility artifacts in diffusion MRI. Frontiers in Neuroinformatics, 11. https://doi.org/10.3389/fninf.2017.00017

Ware Jr, J. E., Kosinski, M., & Keller, S. D. (1996). A 12-Item Short-Form Health Survey: construction of scales and preliminary tests of reliability and validity. Medical care, 220-233.

Weathers, F. W., Litz, B. T., Keane, T. M., Palmieri, P. A., Marx, B. P., & Schnurr, P. P. (2013). The PTSD Checklist for DSM-5 (PCL-5). Scale available from the National Center for PTSD at www. ptsd. va. gov, 10.

Zhang Y, Brady M, Smith S. Segmentation of brain MR images through a hidden Markov random field model and the expectation-maximization algorithm. IEEE Trans Med Imaging. 2001 Jan;20(1):45–57. doi:10.1109/42.906424.